Engineering Fracture Mechanics Vol. 43, No. 3, pp. 417–430, 1992
Printed in Great Britain.

0013-7944/92 $5.00 + 0.00
Pergamon Press Ltd.

AN ESTIMATION METHOD FOR EVALUATING ENERGY RELEASE RATES OF CIRCUMFERENTIAL THROUGH-WALL CRACKED PIPE WELDS

S. RAHMAN and F. W. BRUST
Engineering Mechanics Department, Battelle, Columbus, OH 43201, U.S.A.

Abstract—A new methodology is proposed to estimate energy release rates of through-wall cracked (TWC) ductile pipe weldments subjected to pure bending loads. It is based on the deformation theory of plasticity, the constitutive law characterized by the Ramberg–Osgood model, and an equivalence criterion incorporating the reduced thickness analogy for simulating system compliance due to the presence of a crack in weld metal. A closed form solution is obtained in terms of elementary functions for approximate evaluation of the J-integral. The method utilizes the material properties of both base and weld metals, which are not considered in the current estimation methods. It is very general and can be applied in the complete range between elastic and fully plastic conditions. Several numerical examples are presented to illustrate the proposed technique. Comparisons of results with reference solutions from the finite element method indicate satisfactory prediction of energy release rates.

1. INTRODUCTION

IT IS NOW well established that elastic–plastic fracture mechanics (EPFM) provide more realistic measures of the fracture behavior of cracked engineering systems. The use of EPFM becomes almost necessary for structural materials with high toughness and low strength which generally undergo extensive plastic deformation around a crack tip. Recent analytical, experimental, and computational studies on this subject indicate that the energy release rate (also known as the J-integral) and crack opening displacement (COD) are the most viable fracture parameters for characterizing crack initiation, stable crack growth, and the subsequent instability in ductile materials [1, 2]. This clearly suggests that global parameters like J and/or COD can be conveniently used to assess structural integrity for both leak-before-break and in-service flaw acceptance criteria in degraded piping systems. It is, however, noted that the parameter J still possesses some theoretical limitations. For example, the Hutchinson–Rice–Rosengren (HRR) singular field [3, 4] may not be valid in the case of a certain amount of crack extension where J ceases to act as an amplifier for this singular field. Nevertheless, the possible error is considered tolerable if the relative amount of crack extension stays within a certain limit and if the elastic unloading and non-proportional plastic loading zones around a crack tip are surrounded by a much larger zone of nearly proportional loading controlled by the HRR field. Under this condition of J dominance, both the onset and limited amount of crack growth can be correlated to the critical values of J and the J–resistance curve, respectively [5].

Evaluation of energy release rates in non-linear elastic bodies is usually performed by (i) numerical analysis and (ii) estimation techniques. Traditionally, a comprehensive numerical study has been based on the sophisticated finite element method (FEM) for non-linear stress analysis. Although several general and special purpose computer codes are currently available for FEM, the inconvenience with regard to its applicability as a practical analysis tool is not of minor nature. The computational effort is still significant even with the recent development of numerical techniques, and industry-standard computational facilities. In addition, the employment of the FEM can be time-consuming and may require a high degree of expertise for its implementation. These issues become particularly significant when numerous deterministic analyses are required in a full probabilistic analysis.

For circumferential through-wall cracked (TWC) cylinders, Kumar *et al.* [6] have compiled a series of FEM solutions for various crack sizes, geometries, and material properties in a handbook form. For any arbitrary new problem, the solution is usually achieved from multiple interpolation between tabulated results. Kanninen and Popelar [7] have summarized some general considerations for developing such simplified yet empirically developed estimation approaches. For elastic–plastic

cracked bodies, several approaches have also been developed for estimating energy release rates. Paris and Tada [8] interpolate the value of J between the known elastic solution and the known rigid plastic solution by using a modified Irwin plastic zone correction to the elastic solution. This method does not include the effects of strain hardening. Later, Klecker *et al.* [9] modified the above method to incorporate strain hardening effects using a semi-empirical approach. Brust [10] has developed an estimation method based on reduced compliance simulation by incorporating an artificial uncracked pipe with varying cross-sectional sizes. This method results in a simple closed form solution for various fracture parameters of interest. Using semi-membrane theory of cylindrical shells, Sanders [11] has developed a Dugdale model for TWC pipes. These solutions are also provided in a closed form in terms of elementary functions. All these simplified methods are, however, primarily developed for flawed pipes with cracks in base metal. Currently, there are no reliable estimation techniques available to evaluate the performance of pipes with cracks in weld metal [12]. The energy release rate J for pipe weldment cases is typically estimated assuming that the entire pipe is made up of all base material. This may provide unconservative results for weldment evaluations [13]. Today, though, predictions are usually made using base metal stress–strain data and weld metal J–resistance curves [14]. This can lead to overly conservative or non-conservative predictions depending on the strength ratio of the base versus weld material.

In this paper, a new methodology is developed to predict the energy release rates of TWC ductile pipe weldments subjected to remote bending loads. The method of analysis is based on (i) the classical deformation theory of plasticity, (ii) the constitutive law characterized by the Ramberg–Osgood model, and (iii) equivalence criteria incorporating a reduced thickness analogy for simulating system compliance due to the presence of a crack in weld metal [12]. The method utilizes the material properties of both base and weld metals. The method is general in the sense that it may be applied in the complete range between elastic and fully plastic conditions. Since it is based on J-tearing theory, it is subject to the usual limitations imposed upon this theory, e.g. proportional loading, etc. As explained earlier, this has the implication that the crack growth must be small, although in practice, J-tearing methodology is used far beyond the limits of its theoretical validity with acceptable results [14]. Several numerical examples are presented to illustrate the proposed technique, which is verified with reference solutions from FEM.

2. THE PIPE WELD CRACK PROBLEM

Consider Fig. 1, which illustrates a typical butt-welded pipe with a circumferential through-wall crack of total angle 2θ. The pipe mean radius R and thickness t are shown. Figure 2 illustrates the typical geometry for a butt weld in a pipe. Typically, the weld layers are deposited in sequence. The example of Fig. 2 is an actual sequence from a 4-inch (102-mm) diameter Schedule 80 pipe which required seven passes. The welding gives rise to a heat-affected zone (HAZ), which results in material properties different from those in the weld metal or base metal alone. Often, cracks

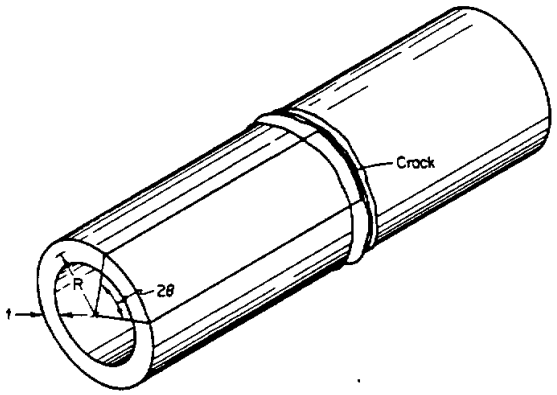

Fig. 1. Circumferential crack in a pipe butt weld.

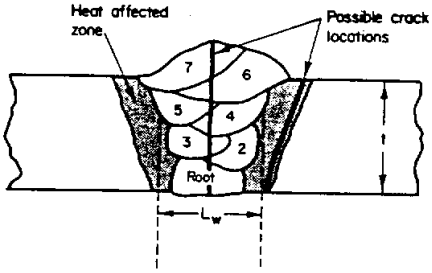

Fig. 2. Typical butt weld sequence for a pipe and possible cracks (this is an actual sequence for a 4-in. diameter Schedule 80 pipe).

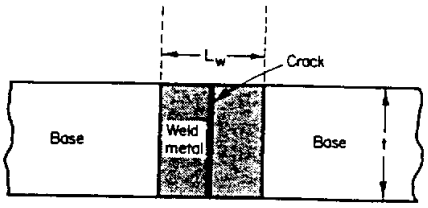

Fig. 3. Idealized pipe weld with a crack.

develop in the HAZ of pipe and may grow in a skewed fashion to become a through-wall crack, as also illustrated in Fig. 2. Figure 2 also shows a crack which grows through the weld metal, and this is the type of crack assumed in the development of the method presented here. Figure 3 shows the pipe weld geometric assumption made here. Note that the angular and irregular nature of the actual weldment is assumed to be a straight radial bimaterial interface line for development of this model. Residual stresses and altered HAZ properties are not included, although they could be considered with rather minor modifications. The total length of the weldment is assumed to be an average (Figs 2 and 3) length, L_w, which is often best approximated (as a rule of thumb) to be the pipe wall thickness (i.e. $L_w \approx t$).

3. GENERAL BACKGROUND

Consider a simply supported TWC pipe under remote bending moment M in Fig. 4 which has length L, mean radius R, thickness t, and crack angle 2θ, with the crack circumferentially located in the weld material of length L_w. In the development of a J-estimation scheme, it is generally assumed that the load point rotation due to the presence of a crack, ϕ^c, and the crack driving force, J, admit additive decomposition of the elastic and plastic components:

$$\phi^c = \phi^c_e + \phi^c_p \tag{1}$$

$$J = J_e + J_p, \tag{2}$$

where the subscripts "e" and "p" refer to the elastic and plastic contributions respectively. In the elastic range, ϕ^c_e and M are uniquely related. In addition, if the deformation theory of plasticity holds, a unique relationship also exists between ϕ^c_p and M. Once these relationships are determined, the elastic component J_e and the plastic component J_p of the total energy release rate J can be readily obtained.

4. ELASTIC SOLUTION

The elastic energy release rate J_e can be defined as

$$J_e = \frac{\partial U^T}{\partial A} = \frac{\partial}{\partial A}(U^c + U^{nc}) = \frac{\partial U^c}{\partial A}, \tag{3}$$

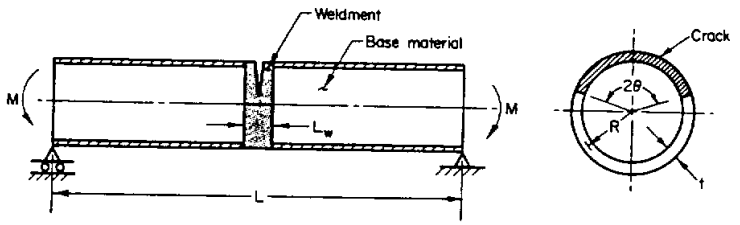

Fig. 4. Schematics of pipe weldments with a circumferential flaw.

where U^T is the total internal strain energy, U^{nc} is the strain energy which would exist if there were no crack present, $U^c = U^T - U^{nc}$ is the additional strain energy in the pipe due to the presence of a crack, and $A = 2R\theta t$ is the crack area. When $t \to 0$, i.e. for a thin-walled pipe with mode I crack growth, J_e can be obtained as

$$J_e = \frac{K_I^2}{E_2}, \tag{4}$$

where E_2 is the elastic modulus of weld material and K_I is the mode I stress intensity factor. From the theory of linear elastic fracture mechanics (LEFM), K_I is given by

$$K_I = \sigma\sqrt{(\pi R\theta)}F_B(\theta), \tag{5}$$

in which $\sigma = M/\pi R^2 t$ is the far-field applied stress and $F_B(\theta)$ is a geometry function relating K_I of a cracked shell to that for the same size of crack in an infinite plate. From eqs (3)–(5), U^c can be integrated to yield

$$U^c = \frac{M^2}{2\pi R^2 t E_2} I_B(\theta), \tag{6}$$

where

$$I_B(\theta) = 4\int_0^\theta \xi F_B(\xi)^2 \, d\xi. \tag{7}$$

Using Castigliano's theorem,

$$\phi_e^c = \frac{\partial U^c}{\partial M}, \tag{8}$$

which when combined with eq. (6) gives

$$M = \frac{E_2 \pi R^2 t}{I_B(\theta)} \phi_e^c, \tag{9}$$

representing the relationship between moment and elastic rotation. Equations (4) and (5) completely specify the elastic energy release rate J_e, and hence the elastic solution is complete in a closed form. Equation (9) provides the relationship between applied moment M and elastic rotation ϕ_e^c which will be required for the calculation of J_p explained in the next section. These developments are based on the elastic solutions of Sanders [15, 16]. Explicit functional forms of $F_B(\theta)$ and $I_B(\theta)$ are provided in Appendix A.

5. PLASTIC SOLUTION

The plastic energy release rate J_p can be defined as

$$J_p = -\int_0^{\phi_p^c} \left.\frac{\partial M}{\partial A}\right|_\zeta d\zeta, \tag{10}$$

where ζ is a dummy variable representing instantaneous plastic rotation. The evaluation of J_p in eq. (10) requires determination of the M–ϕ_p^c relationship as a function of crack size. When this relationship is obtained, eq. (10) can be used to find J_p and can then be added to J_e to determine the total J.

A widely used univariate constitutive law describing a material's stress–strain (σ–ϵ) relation is the normalized Ramberg–Osgood model, given by

$$\frac{\epsilon}{\epsilon_{0i}} = \frac{\sigma}{\sigma_{0i}} + \alpha_i\left(\frac{\sigma}{\sigma_{0i}}\right)^{n_i}, \tag{11}$$

where σ_{0i} is some reference stress usually assumed to be flow stress and/or yield stress, $\epsilon_{0i} = \sigma_{0i}/E_i$ is the associated strain with elastic modulus E_i, α_i and n_i are the model parameters usually chosen to fit experimental data, and $i = 1$ or 2 representing base or weld materials, respectively. In applying the Ramberg–Osgood relation to the cracked pipe problem, it is necessary to relate the stresses with

the rotations. Ilyushin [17] showed that the field solutions to the boundary value problem involving a monotonically increasing load or displacement type parameter are "proportional". Consequently, eq. (11) applies (minus the elastic term) and the deformation theory plasticity is assumed to be valid. Thus,

$$\phi_p^c \propto \sigma^{n_i}, \tag{12}$$

giving

$$\phi_p^c = D\sigma^{n_i}, \tag{13}$$

where the proportionality constant D can be expressed in a convenient form,

$$D = L_B^c \alpha_i \frac{I_B(\theta)}{\sigma_0^{n_i - 1} E_2}, \tag{14}$$

to allow for eq. (13) to be reformulated as

$$\phi_p^c = L_B^c \alpha_i \left(\frac{\sigma}{\sigma_{0i}}\right)^{n_i - 1} \phi_e^c, \tag{15}$$

in which the moment–elastic rotation relationship in eq. (9) is utilized. In eq. (15), L_B^c is an unknown function which needs to be determined. For the crack problem, L_B^c may be determined via a numerical method. However, no analytical method exists to obtain L_B^c in closed form. Thus, the main task in this methodology is to establish L_B^c in eq. (15).

Evaluation of L_B^c

Suppose the actual pipe can be replaced by a pipe with reduced thickness t_e which extends for a distance $\hat{a} \geq L_w$ at the center (Fig. 5). Far from the crack plane, the rotation of the pipe is not greatly influenced by whether a crack exists or some other discontinuity is present as long as the discontinuity can approximate the effects of the crack. The reduced thickness section, which actually results in material discontinuity, is an attempt to simulate the reduced system compliance due to the presence of a crack. This equivalence approach was originally suggested by Brust [10, 18] and successfully implemented to evaluate the performance of TWC pipes consisting of one single material under various loading conditions [10, 18, 19]. It is assumed here that the deformation theory of plasticity controls the stress–strain response and that the beam theory holds.

Consider the equivalent pipe with material discontinuity in Fig. 5 which is subjected to bending load M at both ends. Using classical beam theory, the ordinary differential equations governing displacement of beams with the Ramberg–Osgood constitutive law can be easily derived. These

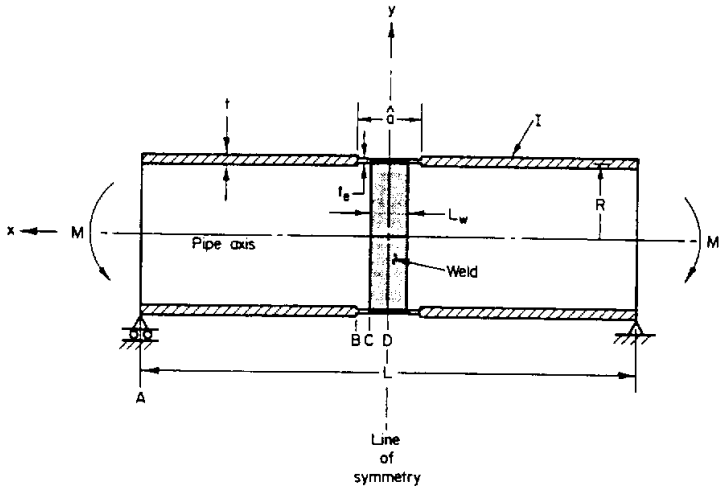

Fig. 5. Reduced section analogy.

equations, when supplemented by the appropriate boundary and compatibility conditions, can be solved following elementary operations of calculus. Details of the algebra associated with these solutions are provided in Appendix B. The rotations [dy/dx in eqs (B2), (B5), and (B8)] provide an explicit relationship between the far-field plastic rotation ϕ_p^d due to material discontinuity and the corresponding elastic rotations ϕ_e^d, where the new superscript "d" refers to material discontinuity. Each of these relationships can be expressed in a form analogous to eq. (15) as

$$\phi_p^d = L_B^d \alpha_i \left(\frac{\sigma}{\sigma_{0i}}\right)^{n_i - 1} \phi_e^d, \tag{16}$$

in which L_B^d in general will depend on geometry, the material properties of base and weld materials, t_e and the spatial coordinate x. While no attempt is made here for a formal proof, it will be assumed that L_B^d determined from the material discontinuity solution [eq. (16)] approaches the actual unknown L_B^c in eq. (15).

Since L_B^d evaluated at segment CD cannot account for base material properties [eq. (B8)], the appropriate choice is to write L_B^d at either segment AB or BC. More specifically, when the spatial location is selected to be the point B (i.e. $x = \hat{a}/2$), the explicit version of eq. (16) becomes

$$\phi_p^d = \frac{\left(\frac{M}{M_{01}}\right)^{n_1}\left(\frac{\hat{a}}{2} - \frac{L_w}{2}\right)\left(\frac{t}{t_e}\right)^{n_1} + \left(\frac{M}{M_{02}}\right)^{n_2}\frac{L_w}{2}\left(\frac{t}{t_e}\right)^{n_2}}{\left(\frac{M}{\bar{M}_1}\right)\epsilon_{01}\left(\frac{\hat{a}}{2} - \frac{L_w}{2}\right)\frac{t}{t_e} + \left(\frac{M}{\bar{M}_2}\right)\epsilon_{02}\frac{L_w}{2}\frac{t}{t_e}} \phi_e^d, \tag{17}$$

where $\bar{M}_i = \sigma_{0i} I/R$ is the elastic bending load corresponding to flow stress σ_{0i}, and the other parameters are already defined in Appendix B. Comparing eq. (17) with eq. (16) immediately gives

$$L_B^d = \frac{\left(\frac{M}{M_{01}}\right)^{n_1}\left(\frac{\hat{a}}{2} - \frac{L_w}{2}\right)\left(\frac{t}{t_e}\right)^{n_1} + \left(\frac{M}{M_{02}}\right)^{n_2}\frac{L_w}{2}\left(\frac{t}{t_e}\right)^{n_2}}{\left(\frac{M}{\bar{M}_1}\right)\epsilon_{01}\left(\frac{\hat{a}}{2} - \frac{L_w}{2}\right)\frac{t}{t_e} + \left(\frac{M}{\bar{M}_2}\right)\epsilon_{02}\frac{L_w}{2}\frac{t}{t_e}} \times \frac{1}{\alpha_1\left(\frac{M}{\bar{M}_1}\right)^{n_1 - 1}}. \tag{18}$$

Equation (18) apparently indicates that L_B^d has explicit functional dependency on the external load parameter M, thus violating the previously invoked Ilyushin theorem [cf. eq. (12)]. However, it can be shown that for the variation of load magnitude in the practical range, the correlation between L_B^d and M is not of strong nature. This will be proved semi-empirically when this issue is further investigated in the forthcoming numerical applications. Hence, the above equation can still be treated as an expression for the invariant proportionality factor L_B^d.

Determination of t_e

The equivalent reduced thickness t_e can be obtained by forcing the limit moment of reduced pipe section,

$$M_L^d = 4\sigma_{\text{limit}} R^2 t_e, \tag{19}$$

to be equivalent to the limit moment of cracked pipe section,

$$M_L^c = 4\sigma_{\text{limit}} R^2 t\left(\cos\frac{\theta}{2} - \frac{1}{2}\sin\theta\right), \tag{20}$$

giving [10, 18]

$$t_e = t\left(\cos\frac{\theta}{2} - \frac{1}{2}\sin\theta\right), \tag{21}$$

which does not require any explicit description of the limit stress σ_{limit} due to its cancellation in the equality of eqs (19) and (20). However, in ref. [10], it has been observed that eq. (21) provides fairly good approximation only for small crack angles ($0° \leqslant 2\theta \leqslant 90°$). For large crack angles ($2\theta \geqslant 120°$), t_e is found to be better represented by

$$t_e = \frac{4}{\pi} t\left(\cos\frac{\theta}{2} - \frac{1}{2}\sin\theta\right), \tag{22}$$

obtained when the limit moment of the reduced section pipe is calculated from the linear stress variation with maximum stress σ_{limit} (giving $M_L^d = \pi\sigma_{limit} R^2 t_e$) rather than a uniform stress block as assumed in eqs (19) and (20). For cracks with angles in the intermediate range ($90° \leqslant 2\theta \leqslant 120°$), t_e can be found by linear interpolation between these limits [10, 18].

Estimation of J_p

Having determined L_B^d and t_e, the M–ϕ_p^c relationship can be obtained from eq. (16) via the M–ϕ_e^c relation in eq. (9). When it is placed in eq. (10), it can be integrated out symbolically to evaluate J_p in a closed form. Following simple algebra, it can be shown that

$$J_p = \frac{\alpha_1}{E\sigma_{01}^{n_1-1}} \frac{1}{n_1+1} \frac{\pi R}{2} H_B L_B^d I_B \left[\frac{M}{\pi R^2 t}\right]^{n_1+1}, \tag{23}$$

in which

$$H_B = \frac{1}{I_B}\frac{\partial I_B}{\partial \theta} + \frac{1}{L_B^d}\frac{\partial L_B^d}{\partial \theta}, \tag{24}$$

where the derivatives $\partial I_B/\partial\theta$ and $\partial L_B^d/\partial\theta$ are explicitly described in Appendix C. Equations (4) and (23) provide closed form expressions for J_e and J_p. These analytic forms are very convenient for both deterministic and probabilistic elastic–plastic fracture mechanics.

6. NUMERICAL EXAMPLES

Description of the problem

Consider two circumferential TWC pipe weldments, one with $R = 52.87$ mm and $t = 8.56$ mm ($R/t \simeq 6$), and the other with $R = 55.88$ mm and $t = 3.81$ mm ($R/t \simeq 15$), each of which is subjected to constant bending moment M applied at the simply supported ends. In both pipes, it is assumed that $2\theta = 139°$ and $L_w = 5.59$ mm. The constitutive laws for base and weld metals are assumed to follow the Ramberg–Osgood model. The numerical values of flow stress σ_{0i}, modulus of elasticity E_i, and the model parameters α_i and n_i are shown in Table 1.

Results of analyses

The pipes with the above input parameters are analyzed to calculate energy release rates (J-integrals) by both the estimation method and the non-linear finite element method (FEM). Approximate evaluation of the crack driving force J by the proposed estimation scheme is based on eqs (2), (4) and (23). The FEM solutions, on the other hand, are based on three-dimensional brick elements available in the fracture mechanics code BCLFEM, which was developed by in-house expertise of the computational group at Battelle. Figure 6 shows a typical mesh representing the finite element idealization of the quarter (due to symmetry) of TWC pipe with cracked weld.

Figures 7 and 8 show several plots of J versus M obtained from various levels of approximation for both pipes with $R/t \simeq 6$ and $R/t \simeq 15$, respectively. Also shown in the figures are the results of the finite element method (FEM), which can be used as benchmark solutions for evaluating the accuracy of analytical methods. Comparisons of the results of the approximate method developed in ref. [18] solely based on all-base or all-weld material properties with those of FEM suggest that they provide only upper and lower bounds of the actual energy release rate J at any given load M. However, neither of them can be used to predict the actual values of J reliably.

Table 1. Parameters of the Ramberg–Osgood model

Material (i)	σ_{0i} (MPa)	E_i (MPa)	α_i	n_i
Base metal	303.3	175,760	30.56	3.826
Weld metal	358.5	175,760	11.96	9.370

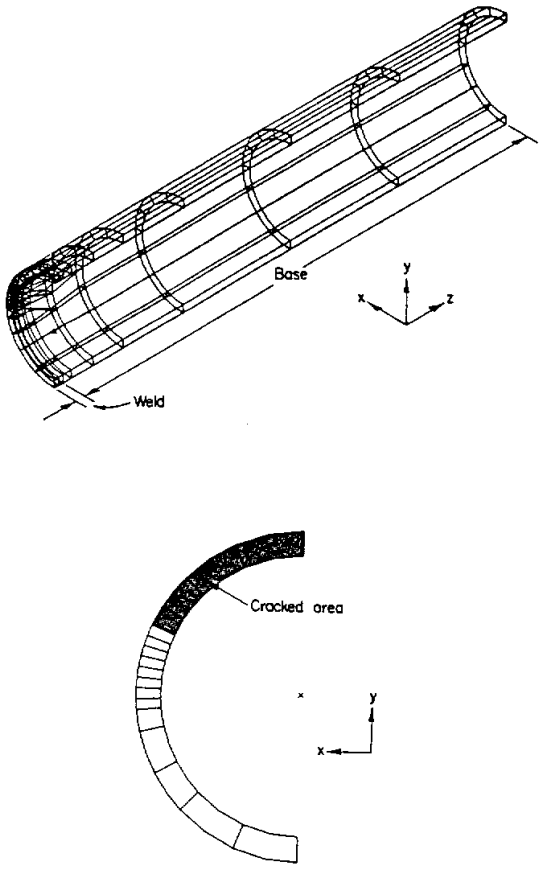

Fig. 6. Finite element mesh of cracked pipe weld.

Figures 7 and 8 also exhibit the results of the proposed method for several values of $\hat{a}$, representing the length of the reduced thickness section. They all show reasonably good agreement with the solutions of FEM. Although $\hat{a}$ is treated here as a free parameter, an optimum value $\hat{a}_{opt}$ needs to be determined for obtaining the best estimate.

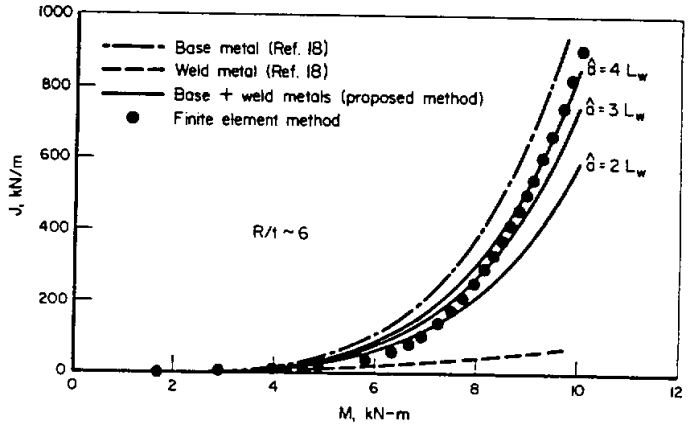

Fig. 7. Comparisons of computed J versus $M(R/t \simeq 6)$.

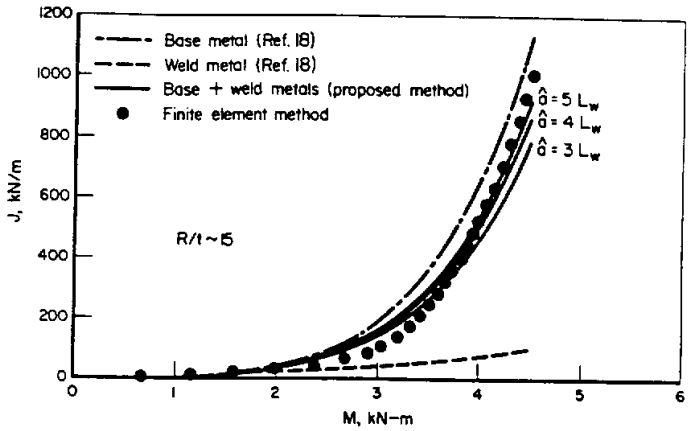

Fig. 8. Comparisons of computed J versus $M(R/t \simeq 15)$.

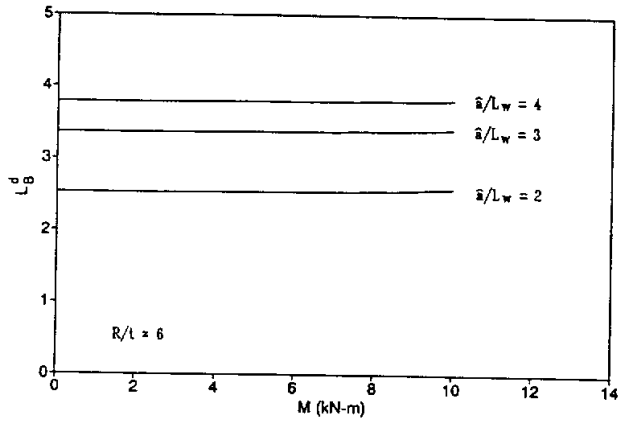

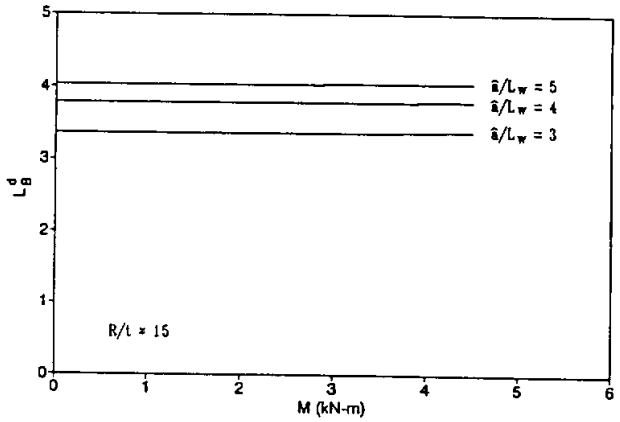

Fig. 9. Plots of L_B^d versus M.

In all the example cases, the calculation of J_p is performed here based on the proportionality factor L_B^d in eq. (18). Although functionally dependent on the external load parameter, the weak correlation between L_B^d and M can be verified from the approximate constancy of L_B^d demonstrated in Fig. 9. This shows several plots of L_B^d versus applied moment M [eq. (18)] for both cases of $R/t \simeq 6$ and $R/t \simeq 15$ in the above examples. As previously anticipated, they clearly indicate that for practical load ranges, L_B^d remains essentially invariant for various combinations of $\hat{a}$.

Quantification of $\hat{a}_{opt}$

Several finite element analyses are carried out to determine the optimum value of $\hat{a}$. Following extensive comparisons with the results of finite element analysis, the optimum value $\hat{a}_{opt}$ is found to be relatively insensitive to the variations in the hardening parameters n_1 and n_2 of the Ramberg–Osgood models for the base and weld metals, respectively. It is also found that the optimum value of $\hat{a}_{opt}/L_w$ is roughly in the neighborhood of 4, where L_w is the average length of weld metal in the pipe.

Figure 10 shows plots of crack driving force J versus applied bending moment M for some of the combinations of n_1 and n_2 considered in this study. Other input parameters are kept the same as in the example problem with $R/t \simeq 6$ illustrated previously. Both estimation and finite element methods are applied to compute J for a given applied moment. Comparisons of the results suggest that the estimation method with the calibrated value of $\hat{a}_{opt}/L_w = 4$ provides simple yet satisfactory measures of the energy release rate J.

Note that the calibration procedure conducted here provides only a preliminary estimate of $\hat{a}_{opt}$. More refined calibration will need to be performed to investigate dependency on geometry

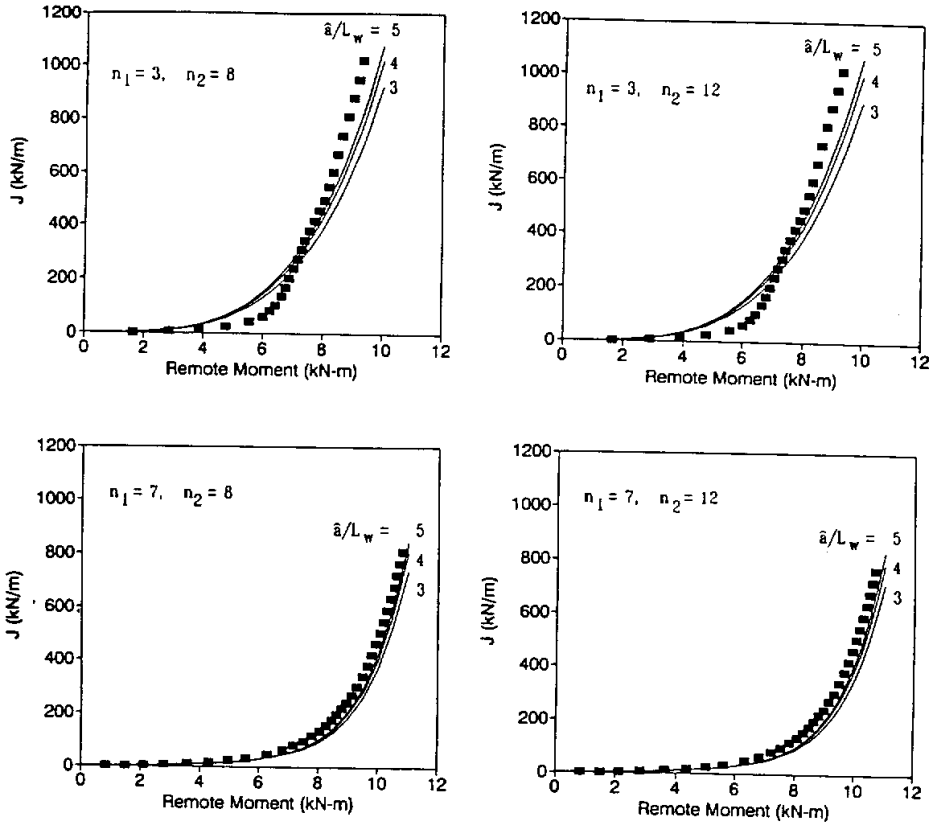

Fig. 10. Numerical calibration of $\hat{a}$. —— estimation methods; ■ finite element analysis.

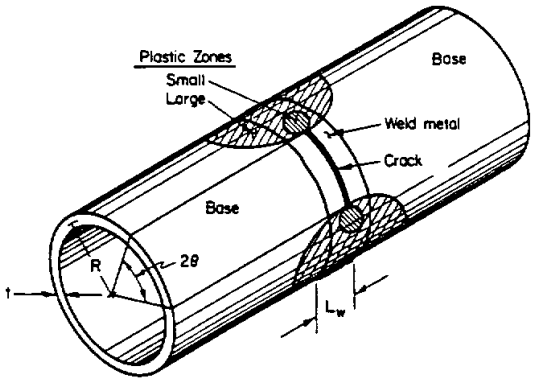

Fig. 11. Circumferential through-wall crack in a weld showing plastic zone sizes.

factor (e.g. R/t ratio), crack size (e.g. θ/π ratio), flow stress ratio (e.g. σ_{01}/σ_{02}), and any other pertinent parameters.

7. DISCUSSION

As discussed here and in refs [10], [18] and [19], the key to developing a J-estimation scheme is to determine the reduced pipe compliance due to the presence of the crack. The reduced pipe compliance has been estimated in a number of ways including using plastic zone correction methods in elastic solutions [10] and reduced thickness sections as done here. The consequences of this equivalence approach are described in the following.

Figure 11 shows the through-wall crack in the weld of a pipe. If the plastic zone is small in comparison to the weld width, L_w, then it is clear that an estimation scheme solution should depend only on the weld material and the corresponding Ramberg–Osgood properties. However, as the plastic zone reaches and penetrates the base metal, the far-field rotation due to the crack increases (or decreases) depending on the ratio of weld to base metal strength properties. For many welded nuclear pipings, the base metal is of lower strength, and can accommodate more plastic flow compared to the weld metal. This additional softening or plastic flow which occurs in the base metal would not occur if not for the presence of the crack. It is for this reason that the reduced thickness section includes both weld and base material, i.e. the additional rotation due to the crack in the base metal is caused by (weld) crack-induced plasticity.

8. CONCLUSIONS

A new methodology is proposed to estimate the energy release rates of TWC ductile pipe weldments subjected to remote bending loads. The method is based on the deformation theory of plasticity, the constitutive law characterized by the Ramberg–Osgood model, and an equivalence criterion incorporating the reduced thickness analogy for simulating system compliance due to the presence of a crack in a weld metal. The method utilizes the material properties of both base and weld metals, which are not considered in the current estimation methods. The method is very general and it can be applied in the complete range between elastic and fully plastic conditions.

Several numerical examples have been presented to illustrate the proposed technique for estimating the J-integral. Similar results from stress analysis based on finite element analysis are also obtained to provide reference solutions for the above problems. Comparison of the results predicted by this new method to the finite element analyses indicated very good predictions of energy release rates.

The equations for the J-integral in a non-linearly elastic cracked pipe weld are derived in a closed form in terms of elementary functions. This makes the proposed scheme computationally feasible and attractive for future development of probabilistic fracture mechanics by both analytical and simulation models. These developments are the subject of current work.

Acknowledgements—The authors would like to thank Dr. Gery Wilkowski of Battelle and Messrs. Michael Mayfield and Allen Hiser of USNRC for their encouragement and support during this effort.

REFERENCES

[1] J. R. Rice, A path-independent integral and the approximate analysis of strain concentration by notches and cracks. *J. appl. Mech.* **35,** 376–386 (1968).
[2] J. W. Hutchinson, Fundamentals of the phenomenological theory of nonlinear fracture mechanics. *J. appl. Mech.* **49,** 103–197 (1982).
[3] J. R. Rice and G. F. Rosengren, Plane strain deformation near a crack-tip in a power-law hardening material. *J. Mech. Phys. Solids* **16,** 1–12 (1968).
[4] J. W. Hutchinson, Singular behavior at the end of a tensile crack in a hardening material. *J. Mech. Phys. Solids* **16,** 13–31 (1968).
[5] P. C. Paris, H. Tada, A. Zahoor and H. Ernst, The theory of instability of the tearing mode of the elastic–plastic crack growth. *Elastic–Plastic Fracture, ASTM STP* **668,** 5–36 (1979).
[6] V. Kumar, M. German, W. Wilkening, W. Andrews, W. deLorenzi and D. Mowbray, Advances in elastic–plastic fracture analysis. EPRI/NP-3607, Final Report (1984).
[7] M. Kanninen and C. Popelar, *Advanced Fracture Mechanics*. Oxford University Press, New York (1985).
[8] P. C. Paris and H. Tada, The application of fracture proof design methods using tearing instability theory to nuclear piping postulating circumferential through-wall cracks. NUREG/CR-3464 (1983).
[9] R. Klecker *et al.*, NRC leak-before-break (LBB.NRC) analysis method for circumferentially through-wall cracked pipes under axial plus bending loads. NUREG/CR-4572 (1986).
[10] F. W. Brust, Approximate methods for fracture analysis of through-wall cracked pipes. NUREG/CR-4853 (1987).
[11] J. L. Sanders, Jr., Dugdale model for circumferential through-cracks in pipes loaded by bending. *Int J. Fracture* **34,** 71–81 (1987).
[12] S. Rahman, F. Brust, M. Nakagaki and P. Gilles, An approximate method for estimating energy release rates of through-wall cracked pipe weldments. *Proc.* 1991 *ASME Pressure Vessels and Piping Conf.*, Vol. 215, San Diego, CA (1991).
[13] *Proc. CSNI/NRC Workshop on Ductile Piping Fracture Mechanics* (Compiled by M. F. Kanninen), held at the Southwest Research Institute, San Antonio, TX (1984).
[14] G. M. Wilkowski *et al.*, Degraded piping program—Phase II. NUREG/CR-4082, Final and Semiannual Reports (1985–1989).
[15] J. L. Sanders, Jr., Circumferential through-cracks in cylindrical shells under tension. *J. appl. Mech.* **49,** 103–107 (1982).
[16] J. L. Sanders, Jr., Circumferential through-crack in a cylindrical shell under combined bending and tension. *J. appl. Mech.* **50,** 221 (1983).
[17] A. A. Ilyushin, The theory of small elastic–plastic deformations. *Prikadnaia Matematika i Mekhanika, PMM* **10,** 347–356 (1946).
[18] F. W. Brust and P. Gilles, An equivalence method for estimating energy release rates with application to cracked cylinders. *J. Press. Vess. Technol.* (in press).
[19] P. Gilles and F. W. Brust, Approximate methods for fracture analysis of tubular members subjected to combined tensile and bending loads. *Proc. 8th OMAE Conf.*, The Hague, The Netherlands (1989).

APPENDIX A

Using Sanders' solutions [15, 16] by shell theory and the energy integral technique, Paris and Tada [8] have developed the following approximations of $F_B(\theta)$ and $I_B(\theta)$:

$$F_B(\theta) \simeq 1 + A_b\left(\frac{\theta}{\pi}\right)^{1.5} + B_b\left(\frac{\theta}{\pi}\right)^{2.5} + C_b\left(\frac{\theta}{\pi}\right)^{3.5} \tag{A1}$$

with

$$\begin{aligned} A_b &= -3.2654 + 1.5278\left(\frac{R}{t}\right) - 0.0727\left(\frac{R}{t}\right)^2 + 0.0016\left(\frac{R}{t}\right)^3 \\ B_b &= 11.3632 - 3.9141\left(\frac{R}{t}\right) + 0.1862\left(\frac{R}{t}\right)^2 - 0.0041\left(\frac{R}{t}\right)^3 \\ C_b &= -3.1861 + 3.8476\left(\frac{R}{t}\right) - 0.1830\left(\frac{R}{t}\right)^2 + 0.0040\left(\frac{R}{t}\right)^3 \end{aligned} \tag{A2}$$

and

$$I_B(\theta) \simeq 2\theta^2\left[1 + 8\left(\frac{\theta}{\pi}\right)^{1.5} I_{b_1} + \left(\frac{\theta}{\pi}\right)^3 (I_{b_2} + I_{b_3})\right], \tag{A3}$$

where

$$\begin{aligned} I_{b_1} &= \frac{A_b}{7} + \frac{B_b}{9}\left(\frac{\theta}{\pi}\right) + \frac{C_b}{11}\left(\frac{\theta}{\pi}\right)^2 \\ I_{b_2} &= \frac{A_b^2}{2.5} + \frac{A_b B_b}{1.5}\left(\frac{\theta}{\pi}\right) + \frac{2A_bC_b + B_b^2}{3.5}\left(\frac{\theta}{\pi}\right)^2 \\ I_{b_3} &= \frac{B_bC_b}{2}\left(\frac{\theta}{\pi}\right)^3 + \frac{C_b^2}{4.5}\left(\frac{\theta}{\pi}\right)^4. \end{aligned} \tag{A4}$$

APPENDIX B

Using classical beam theory for small deformation, the governing differential equations are (Fig. 5):

1. Segment AB ($\hat{a}/2 \leqslant x \leqslant L/2$)

$$\frac{d^2y}{dx^2} = \frac{1}{R}\left(\frac{M}{M_{01}}\right)^{n_1} \tag{B1}$$

$$\frac{dy}{dx} = \frac{1}{R}\left(\frac{M}{M_{01}}\right)^{n_1} x + C_1 \tag{B2}$$

$$y = \frac{1}{R}\left(\frac{M}{M_{01}}\right)^{n_1} \frac{x^2}{2} + C_1 x + C_2 \tag{B3}$$

2. Segment BC ($L_w/2 \leqslant x \leqslant \hat{a}/2$)

$$\frac{d^2y}{dx^2} = \frac{1}{R}\left(\frac{M}{M_{01}}\right)^{n_1}\left(\frac{t}{t_e}\right)^{n_1} \tag{B4}$$

$$\frac{dy}{dx} = \frac{1}{R}\left(\frac{M}{M_{01}}\right)^{n_1}\left(\frac{t}{t_e}\right)^{n_1} x + C_3 \tag{B5}$$

$$y = \frac{1}{R}\left(\frac{M}{M_{01}}\right)^{n_1}\left(\frac{t}{t_e}\right)^{n_1} \frac{x^2}{2} + C_3 x + C_4 \tag{B6}$$

3. Segment CD ($0 \leqslant x \leqslant L_w/2$)

$$\frac{d^2y}{dx^2} = \frac{1}{R}\left(\frac{M}{M_{02}}\right)^{n_2}\left(\frac{t}{t_e}\right)^{n_2} \tag{B7}$$

$$\frac{dy}{dx} = \frac{1}{R}\left(\frac{M}{M_{02}}\right)^{n_2}\left(\frac{t}{t_e}\right)^{n_2} x + C_5 \tag{B8}$$

$$y = \frac{1}{R}\left(\frac{M}{M_{02}}\right)^{n_2}\left(\frac{t}{t_e}\right)^{n_2} \frac{x^2}{2} + C_5 x + C_6, \tag{B9}$$

where

$$M_{0i} = \frac{4K_i I \hat{K}_i}{\pi R} \tag{B10}$$

with

$$K_i = \frac{\sigma_{0i}}{(\alpha_i \epsilon_{0i})^{1/n_i}} \tag{B11}$$

$$\hat{K}_i = \frac{\sqrt{\pi}}{2}\frac{\Gamma\left(1+\frac{1}{2n_i}\right)}{\Gamma\left(\frac{3}{2}+\frac{1}{2n_i}\right)} \tag{B12}$$

and the gamma function

$$\Gamma(u) = \int_0^\infty \xi^{u-1}\exp(-\xi)\,d\xi, \tag{B13}$$

in which $I \simeq \pi R^3 t$ is the moment of inertia of the original pipe cross-section. Enforcing the appropriate boundary and compatibility conditions, the constants C_1–C_6 can be easily determined as

$$C_1 = -\frac{1}{R}\left(\frac{M}{M_{01}}\right)^{n_1}\left[\frac{\hat{a}}{2}\left\{1-\left(\frac{t}{t_e}\right)^{n_1}\right\} + \frac{L_w}{2}\left(\frac{t}{t_e}\right)^{n_1}\right] + \frac{1}{R}\left(\frac{M}{M_{02}}\right)^{n_2}\left[\frac{L_w}{2}\left(\frac{t}{t_e}\right)^{n_2}\right] \tag{B14}$$

$$C_2 = \frac{1}{R}\left(\frac{M}{M_{01}}\right)^{n_1}\left[-\frac{L^2}{8} + \frac{L}{2}\frac{\hat{a}}{2}\left\{1-\left(\frac{t}{t_e}\right)^{n_1}\right\} + \frac{L}{2}\frac{L_w}{2}\left(\frac{t}{t_e}\right)^{n_1}\right] - \frac{1}{R}\left(\frac{M}{M_{02}}\right)^{n_2}\left[\frac{L}{2}\frac{L_w}{2}\left(\frac{t}{t_e}\right)^{n_2}\right] \tag{B15}$$

$$C_3 = -\frac{1}{R}\left(\frac{M}{M_{01}}\right)^{n_1}\left[\frac{L_w}{2}\left(\frac{t}{t_e}\right)^{n_1}\right] + \frac{1}{R}\left(\frac{M}{M_{02}}\right)^{n_2}\left[\frac{L_w}{2}\left(\frac{t}{t_e}\right)^{n_2}\right] \tag{B16}$$

$$C_4 = \frac{1}{R}\left(\frac{M}{M_{01}}\right)^{n_1}\left[-\frac{L^2}{8} + \frac{L}{2}\frac{\hat{a}}{2}\left\{1-\left(\frac{t}{t_e}\right)^{n_1}\right\} + \frac{L}{2}\frac{L_w}{2}\left(\frac{t}{t_e}\right)^{n_1} - \frac{\hat{a}^2}{8}\right] - \frac{1}{R}\left(\frac{M}{M_{02}}\right)^{n_2}\left[\frac{L}{2}\frac{L_w}{2}\left(\frac{t}{t_e}\right)^{n_2}\right] \tag{B17}$$

$$C_5 = 0 \tag{B18}$$

$$C_6 = \frac{1}{R}\left(\frac{M}{M_{01}}\right)^{n_1}\left[-\frac{L^2}{8} + \frac{L}{2}\frac{\hat{a}}{2}\left\{1-\left(\frac{t}{t_e}\right)^{n_1}\right\} + \frac{L}{2}\frac{L_w}{2}\left(\frac{t}{t_e}\right)^{n_1} - \frac{\hat{a}^2}{8} - \frac{L_w^2}{8}\left(\frac{t}{t_e}\right)^{n_1}\right] - \frac{1}{R}\left(\frac{M}{M_{02}}\right)^{n_2}\left[\frac{L_w^2}{8}\left(\frac{t}{t_e}\right)^{n_2} - \frac{L}{2}\frac{L_w}{2}\left(\frac{t}{t_e}\right)^{n_2}\right]. \tag{B19}$$

APPENDIX C

The expressions for the derivatives $\partial I_B/\partial\theta$ and $\partial L_B^d/\partial\theta$ are given below:

$$\frac{\partial I_B}{\partial\theta} = 4\theta F_B(\theta)^2 \tag{C1}$$

$$\frac{\partial L_B^d}{\partial\theta} = \frac{A_3 G_1(\theta)[A_1 G'_{n_1}(\theta) + A_2 G'_{n_2}(\theta)] - A_3 G'_1(\theta)[A_1 G_{n_1}(\theta) + A_2 G_{n_2}(\theta)]}{[A_3 G_1(\theta)]^2}, \tag{C2}$$

in which

$$G_k(\theta) = \left(\cos\frac{\theta}{2} - \frac{1}{2}\sin\theta\right)^{-k}$$

$$G'_k(\theta) = \frac{k}{2}\left(\sin\frac{\theta}{2} + \cos\theta\right)G_{k+1}(\theta) \tag{C3}$$

$$A_1 = \left(\frac{M}{M_{01}}\right)^{n_1}\left[\frac{\hat{a}}{2} - \frac{L_w}{2}\right]C^{-n_1}\frac{1}{\alpha_1\left(\dfrac{M}{M_1}\right)^{n_1-1}}$$

$$A_2 = \left(\frac{M}{M_{02}}\right)^{n_2}\left[\frac{L_w}{2}\right]C^{-n_2}\frac{1}{\alpha_1\left(\dfrac{M}{M_1}\right)^{n_1-1}}$$

$$A_3 = \left(\frac{M}{M_1}\right)\epsilon_{01}\left[\frac{\hat{a}}{2} - \frac{L_w}{2}\right]C^{-1} + \left(\frac{M}{M_2}\right)\epsilon_{02}\left[\frac{L_w}{2}\right]C^{-1}, \tag{C4}$$

where $C = 1$ or $C = 4/\pi$ according to whether $0^\circ \leqslant 2\theta \leqslant 90^\circ$ or $2\theta \geqslant 120^\circ$, respectively. When $90^\circ \leqslant 2\theta \leqslant 120^\circ$, C can be interpolated from the above two limits [10, 18].

(*Received* 9 *September* 1991)